Localization, delocalization, and topological transitions in disordered two-dimensional quantum walks

Jonathan M. Edge[1] and Janos K. Asboth[2]

[1]*Nordita, KTH Royal Institute of Technology and Stockholm University, Roslagstullsbacken 23 106 91 Stockholm, Sweden*

[2]*Institute for Solid State Physics and Optics, Wigner Research Centre, Hungarian Academy of Sciences, H-1525 Budapest P.O. Box 49, Hungary*

(Received 2 December 2014; revised manuscript received 16 February 2015; published 5 March 2015)

We investigate time-independent disorder on several two-dimensional discrete-time quantum walks. We find numerically that, contrary to claims in the literature, random onsite phase disorder, spin-dependent or otherwise, cannot localize the Hadamard quantum walk; rather, it induces diffusive spreading of the walker. In contrast, split-step quantum walks are generically localized by phase disorder. We explain this difference by showing that the Hadamard walk is a special case of the split-step quantum walk, with parameters tuned to a critical point at a topological phase transition. We show that the topological phase transition can also be reached by introducing strong disorder in the rotation angles. We determine the critical exponent for the divergence of the localization length at the topological phase transition, and find $\nu = 2.6$, in both cases. This places the two-dimensional split-step quantum walk in the universality class of the quantum Hall effect.

DOI: 10.1103/PhysRevB.91.104202 PACS number(s): 73.43.Nq, 05.40.Fb, 03.67.Ac

Discrete-time quantum walks [1], which we will simply refer to as quantum walks, are the quantum analogs of classical random walks. They are model systems which sit at the interface between quantum information theory and condensed matter physics. On the one hand, they form archetypical systems for studying quantum algorithms [2,3]. On the other hand, condensed matter physics has recently also shown interest in quantum walks [4–6] in particular ever since it was shown that the topological phases [7,8] can also be realized in quantum walks [9].

Condensed matter physics has a very wide scope, but one important subject of it is disorder and the associated localization of single-particle wave functions (for a review, see Ref. [10]). Thus, to understand quantum walks from the condensed matter point of view, we need to address the effect of disorder on the propagation of a quantum walker.

One of the interesting aspects of quantum walks is that in the absence of disorder, the quantum walker propagates ballistically [1], thus much faster than its classical counterpart, which shows diffusive propagation. The ballistic spreading of the quantum walk is related to the quantum speedup of certain quantum algorithms, notably Grover's search algorithm [11], as the quantum walker is able to explore the search space more rapidly than its classical counterpart.

If disorder is introduced into the quantum walk system, it is expected to break the ballistic propagation of the quantum walk, analogously to the way in which disorder introduced into a solid-state system will affect electrons due to disorder scattering. This could be of relevance to the quantum information applications of quantum walks, as the quantum speedup of quantum algorithms is intimately related to ballistic propagation.

Although the effects of disorder on one-dimensional quantum walks have been extensively studied, not much is known about the two-dimensional case. For one-dimensional quantum walks, it has been shown that spatial disorder can lead to exponential localization of all energy eigenstates [12–16]. It was also found, however, that chiral symmetry can prevent localization in one dimension [5]. To the best of our knowledge, the effects of spatial disorder in two-dimensional quantum walks and its impact on the quantum walk propagation was only studied in Ref. [17] for the Hadamard walk. In that paper it was reported that in the disordered system the wave function remains majoritatively close to the starting position, unlike in the clean case, where the amplitude of the wave function at the initial site decreases to zero in the long-time limit. This concentration of the wave function close to its initial position (which is according to a looser terminology used as the definition of localization, as, e.g, in Ref. [18]) was attributed to Anderson localization.

In this paper, we study the effects of spatial disorder on the propagation and localization of the Hadamard walk, and on the broader family of two-dimensional split-step walks to which it belongs. Section I collects the definitions of these walks, recalls their connection and their topological phases. In Sec. II, we show that phase disorder localizes generic split-step walks, but not the Hadamard walk: the latter shows slow diffusion (contrary to the findings of Ref. [17]). In Sec. III, we attribute this difference to the fact that the Hadamard walk is critical: it is a split-step walk that is tuned to a topological phase transition point. We demonstrate this phase transition and calculate the corresponding critical exponent $\nu = 2.6$, which places the split-step walk in the quantum Hall universality class. Finally, in Sec. IV we study disorder in the angle parameters of the split-step walks. Based on the preceding section, one can expect that if the angle disorder is large enough, the split-step walk can become diffusive even with maximal phase disorder. We show that this disorder-induced delocalization actually takes place, and find for it the same critical exponent ν as in Sec. III. We also find that angle disorder alone leads to diffusion rather than localization, which is probably connected to the presence of a particle-hole symmetry in this disordered quantum walk.

I. DEFINITIONS OF THE QUANTUM WALKS

A particle undergoing a quantum walk on a square lattice is represented by a time-dependent two-component wave

function

$$|\psi(t)\rangle = \sum_{m,n}\sum_{s=\pm1} \psi(t)_{m,n,s}|m,n,s\rangle. \quad (1)$$

Here, $m,n \in \mathbb{Z}$ give the horizontal and vertical positions on the lattice, $s \in \{+1,-1\}$ is the value of the internal state that we call spin, and $t \in \mathbb{N}$ denotes the time, which is only allowed to take on discrete values. We take as initial condition a localized state $|0,0,+1\rangle$ and obtain the time evolution by iterated applications of the time-evolution operator U on the state

$$|\psi(t)\rangle = U^t|0,0,+1\rangle. \quad (2)$$

We will consider different types of quantum walks, with the time-evolution operator U consisting of a product of several shift operators and coin operators, to be defined in the following.

Shift operators displace the walker by one lattice site in a direction that depends on its internal state, but their action is independent of the position of the walker. We consider the quantum walk on a square lattice with the sites labeled by (m,n) and so define the following shift operators:

$$\hat{S}_x = \sum_{m,n}\sum_{s=\pm1} |m+s,n,s\rangle\langle m,n,s|;$$

$$\hat{S}_y = \sum_{m,n}\sum_{s=\pm1} |m,n+s,s\rangle\langle m,n,s|.$$

We use absorbing boundary conditions [19] in both the x and y directions.

Coin operators act locally on the walker, but can have position-dependent parameters. They can be written in compact form using the Pauli operators $\sigma_z|m,n,s\rangle = s|m,n,s\rangle$, $\sigma_x|m,n,s\rangle = |m,n,-s\rangle$, $\sigma_y|m,n,s\rangle = is|m,n,-s\rangle$, and $\sigma_0|m,n,s\rangle = |m,n,s\rangle$ for all values of m, n, and s. We consider the Hadamard coin operator

$$\hat{H} = 2^{-1/2}(\sigma_x + \sigma_z) \quad (3)$$

and the spin-rotation operator

$$\hat{R}[\theta_j] = \sum_{m,n} e^{-i\theta_j^{mn}\sigma_y}|m,n\rangle\langle m,n|,$$

with θ_j^{mn} denoting the position-dependent rotation angles. The index j differentiates between rotations in one sequence of operations defining the time step; below, the time-evolution operator will contain two spin rotations, and so j will take values 1 and 2. Since $\hat{R}[\theta_j+\pi] = -\hat{R}[\theta_j]$, only angles between $-\frac{\pi}{2}$ and $\frac{\pi}{2}$ give distinct rotation operators (the minus sign is only a phase factor).

The first type of quantum walk we consider is the Hadamard walk, defined through its time-evolution operator

$$U_H = \hat{S}_y\hat{H}\hat{S}_x\hat{H}. \quad (4)$$

It thus consists of a Hadamard coin operation followed by a spin-dependent displacement in the x direction, another Hadamard coin operation rotation and a displacement in the y direction.

We also consider the split-step quantum walk [9], where the time-evolution operator is defined as

$$U_s = \hat{S}_y\hat{R}[\theta_2]\hat{S}_x\hat{R}[\theta_1]. \quad (5)$$

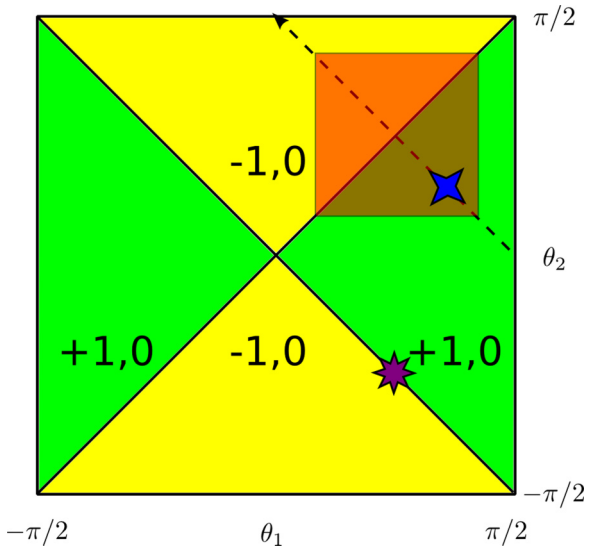

FIG. 1. (Color online) Phase diagram for the topological quantum numbers for the split-step quantum walk defined by Eq. (5) without disorder [19]. As described in Ref. [19], due to the time-periodic nature of the quantum walk, two topological invariants can be defined, only one of which changes in the parameter range under consideration in this paper. The red transparent box shows the range of θ_1 and θ_2 which is accessible at the point $\theta_1 = \theta_2 = \pi/4$ for the parameters in Figs. 4 and 5. The blue four-sided star shows the parameter set $\theta_1 = 0.35\pi$, $\theta_2 = 0.15\pi$ which is frequently used throughout this paper. The purple eight-sided star shows the parameters $\theta_1 = \pi/4$, $\theta_2 = -\pi/4$ at which the split-step quantum walk reduces to the Hadamard walk.

As described in Ref. [19], for rotation angles $\theta_j^{mn} = \theta_j$ independent of position, the system has two topological invariants: the Chern number and the quasienergy winding [20], which are determined by θ_1 and θ_2. The phase diagram for the topological invariants is reproduced in Fig. 1. The Chern number for this quantum walk is always zero, but, as we will see, the quasienergy winding plays an important role in determining the localization properties.

The split-step quantum walk can be seen as a generalization of the Hadamard walk. Since $H = \sigma_x e^{-i(\pi/4)\sigma_y} = e^{i(\pi/4)\sigma_y}\sigma_x$, we have

$$U_H = S_y R(-\pi/4)S_x^{-1}R(\pi/4). \quad (6)$$

Thus, the Hadamard walk is a mirror reflected $x \leftrightarrow -x$ version of the split-step walk, with $\theta_1 = -\theta_2 = \pi/4$.

II. EFFECT OF PHASE DISORDER

One way to introduce discrete-time independent disorder into quantum walks is to multiply the wave function at the end of each time step by a random phase factor, which depends on position and spin value, but not on time. For this, we define the phase operators

$$\hat{P}_a[\phi] = \sum_{m,n} e^{i\phi_{mn}\sigma_a}|m,n\rangle\langle m,n|,$$

with $a = 0$ for a spin-independent and $a = z$ for a spin-dependent phase operator. We take the phases ϕ_{mn} to have

zero mean value, and distributed randomly in the interval $[-\delta\phi/2,\delta\phi/2)$. Intuitively, $\hat{P}_0$ mimics an onsite energy in a tight-binding lattice model, while $\hat{P}_z$ can be understood as a disordered magnetic field. As such, these types of disorder favor localization in noninteracting two-dimensional lattice systems [21].

A. Hadamard walk with phase disorder: Disorder-induced diffusion

To add phase disorder to the Hadamard quantum walk [Eq. (4)], we define the time-step operator as

$$U_{H,a} = \hat{P}_a \hat{S}_y \hat{H} \hat{S}_x \hat{H}. \tag{7}$$

For different values of $\delta\phi$ between 0 and 2π, and different disorder realizations, we initialize the quantum walker at the center of a 220×220 lattice,[1] and follow the time evolution for 1000 time steps.

To detect localization, we will use two of its signatures. First, in the presence of localization, the wave function in the long-time limit should decrease exponentially as a function of the distance from the initial site

$$\sum_{s=\pm 1} |\Psi(t \to \infty)^2_{m,n,s}| \propto e^{-2\sqrt{m^2+n^2}/\xi}. \tag{8}$$

The localization length $\xi \in \mathbb{R}$ of a localized wave function should be well defined (at least in the vicinity of the initial site). Second, in the localized case, the spreading $s(t)$ of the wave function, defined as

$$s^2(t) = \sum_{m,n} \sum_{s=\pm 1} (m^2+n^2)|\Psi(t)_{m,n,s}|^2, \tag{9}$$

should saturate, i.e., $\lim_{t\to\infty} s(t) = \text{const}$.

In the Hadamard walk with phase disorder, we find diffusive dynamics instead of localization. In Fig. 2, we have plotted a cross section of the probability amplitude squared of the wave function after 1000 time steps of both the Hadamard walk with spin-dependent and spin-independent disorder, averaged over 500 disorder realizations. We see that although the wave function is strongly peaked towards the center, it does not decay exponentially: in both cases, it shows a Gaussian profile characteristic of diffusive behavior [22]. The inset shows the spreading $s(t)$, which displays no sign of saturation: it is well approximated by $s(t) \propto t^{1/2}$, which again is an indication of diffusion.

Our results contradict those of Ref. [17], where localization was found for the disordered Hadamard walk, and also go against the intuitive picture that onsite disorder induces localization. Although it cannot, in principle, be ruled out that localization will eventually set in, the 1000 times steps we considered give an already significantly larger time scale than the 20 time steps investigated in Ref. [17]. Why is there no localization in the disordered Hadamard walk? This is one of the main questions which we will answer in the following.

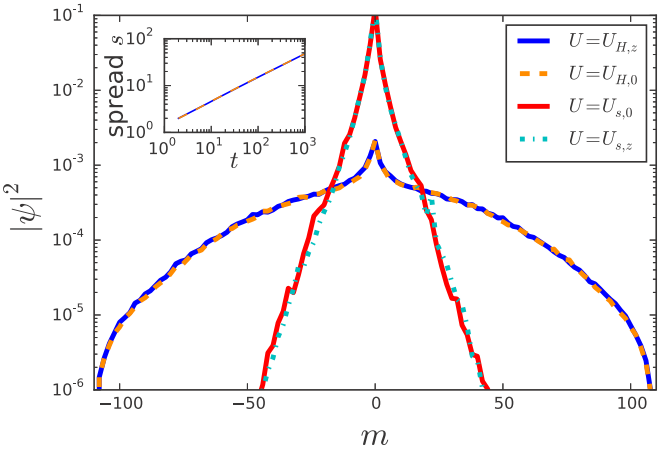

FIG. 2. (Color online) Wave-function cross section at $n = 0$ after 1000 time steps for a quantum walker initialized at the center of a 220×220 lattice, averaged over 500 disorder realizations. Only even lattice sites are shown, as the wave function is zero on odd lattice sites for $t = 1000$. In total, four types of quantum walks are shown: $U_{H,a}$ [Eq. (7)] and $U_{s,a}$ [Eq. (10)] with $a = 0,z$, $\delta\phi = 2\pi$. For $U_{s,a}$ we choose $\theta_1 = 0.35\pi$, $\theta_2 = 0.15\pi$, and $\delta\theta = 0.14\pi$. As we can see, $U_{H,0}$ and $U_{H,z}$ show similar types of diffusive behavior. The inset shows the spreading of the wave function for $U_{H,z}$ and $U_{H,0}$ (same color coding as in the main figure), which is roughly consistent with the diffusive $s \sim \sqrt{t}$ behavior. In contrast, $U_{s,0}$ and $U_{s,z}$ show localizing behavior according to Eq. (8).

B. Split-step walk with phase disorder: Disorder-induced localization

To obtain a full picture of phase disorder and its effects on localization, we now apply disorder to the generic split-step walk, which can be seen as a generalization of the Hadamard walk [cf. Eq. (6)]. We fix the rotation angles at $\theta_1 = 0.35\pi$ and $\theta_2 = 0.15\pi$. As seen on the phase space of the walk, Fig. 1, this set of parameters is far from the continuous lines along which the quasienergy gap closes. The time-evolution operator is then given by

$$U_{s,a} = \hat{P}_a[\phi] S_y R[\theta_2] S_y R[\theta_1], \tag{10}$$

with $a = 0$ for spin-independent and $a = z$ for spin-dependent disorder. We remark that both types of phase disorder break the particle-hole symmetry of the system, which arose since U_s was real [9].

Our numerical results indicate that unlike the Hadamard walk, the two-dimensional (2D) split-step quantum walk is localized by phase disorder. As shown in Fig. 3, in the absence of phase disorder $\delta\phi = 0$, the wave function spreads ballistically, as expected. As $\delta\phi$ is increased, however, the wave function spreads more slowly, and for large values of $\delta\phi$, it seems to saturate indicating localization. The inset of Fig. 3 shows the localization transition through the exponent α obtained by fitting $s(t) \propto t^\alpha$ to the numerical results over short ($10 < t < 100$, green dashed line) and long[2] ($10 < t < 1000$, blue solid line) times. When $\delta\phi = 0$, we observe ballistic

[1] Throughout this paper we choose lattice sizes large enough for the boundary to have no effect.

[2] For small values of disorder, the walker spreads very rapidly, such that it reaches the boundary before $t = 1000$. For these cases, we

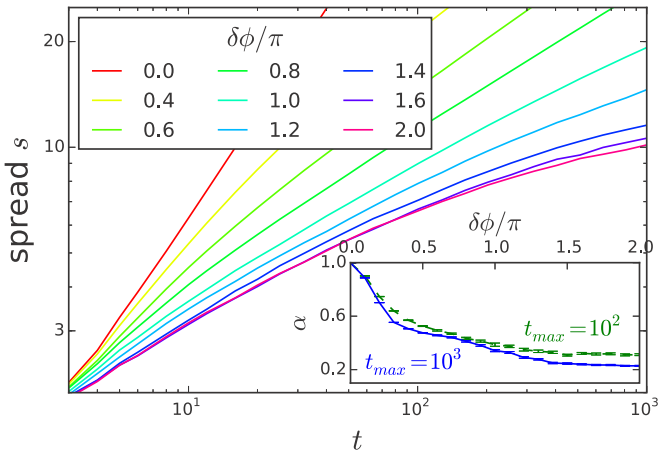

FIG. 3. (Color online) Spreading $s(t)$ of the wave function in the quantum walk $U_{s,0}$ of Eq. (10) as a function of time, with various amounts of phase disorder $\delta\phi$, averaged over 100 disorder realizations (log-log plot). The rotation angle parameters are set to $\theta_1 = 0.35\pi$, $\theta_2 = 0.15\pi$. Upon increasing the phase disorder, the walk shifts from a delocalized $[s(t) \propto t^{\alpha}]$ to a localized $[\lim_{t\to\infty} s(t) = \text{const}]$ behavior. Inset: exponent α of $s(t) \propto t^{\alpha}$ fitted to the curves between $t_{min} = 10$ and $t_{\max}$ (blue solid line: $t_{\max} = 100$, green dashed line: $t_{\max} = 1000$). For $\delta\theta = 0$, the system behaves ballistically, with $\alpha = 1$. For larger disorder, the fitted value of α decreases with time, indicating localization.

propagation, indicated by a time-independent value of $\alpha = 1$. For increasing values of disorder α decreases and, more importantly, decreases as a function of time. This indicates that a power-law fit for $s(t)$ does not provide a good fit and that the system is localizing. Additional evidence for localization is furnished by the shape of the wave function in the long-time limit, as shown in Fig. 2.

III. TOPOLOGICAL TRANSITION BEHIND DELOCALIZATION

The difference in the effects of phase disorder on the Hadamard walk (diffusion) and the generic split-step quantum walk (localization) is due to the fact that the Hadamard walk is a special case of the split-step walk, tuned to a topological phase transition point. In this section, we expand on this explanation, and investigate it numerically, obtaining the critical exponents corresponding to this phase transition via single-parameter scaling.

To make sure that the effect we observe is generic, we also include a small amount of disorder in the angle parameters of the split-step quantum walk. These angles θ_j^{mn} will be chosen randomly and independently for each site, from a uniform distribution in the interval $[\theta_j - \delta\theta, \theta_j + \delta\theta)$. Thus, the first and second rotations have the same disorder $\delta\theta$, which we fix in this section to be $\delta\theta = 0.2\pi$.

have fitted α in the range $10 \leqslant t \leqslant t_{\delta\phi}$ where $t_{\delta\phi}$ is chosen to be a time before the walker has reached the boundary.

A. Topological transition by tuning the mean rotation angles

We locate the topological phase transition by tuning the parameters of the quantum walk: we gradually increase θ_2 from 0 to $\pi/2$ while keeping $\theta_1 + \theta_2 = \pi/2$ constant, all the while keeping maximal phase disorder $\delta\phi = 2\pi$ and a moderate angle disorder $\delta\theta = 0.2\pi$. This path is marked by the dashed line in Fig. 1. We characterize the localization properties for each set of parameter values via the time-dependent diffusion coefficient

$$D(t) = \frac{s^2(t)}{t}. \tag{11}$$

In the long-time limit, the diffusion coefficient $D(t)$ is a constant in regimes governed by diffusion (metallic or possibly critical regimes) and decreases in time in the localized regime (nonmetallic regime). We choose this quantity because it will be a suitable starting point for the scaling analysis of the transition point.

Our results for the diffusion coefficient D for various times, as the rotation angles θ_j are tuned across topological phase transition, are shown in Fig. 4. At most values of the angles, the calculated values of $D(t)$ decrease with time t, and we can infer that the quantum walk is localized. At the point $\theta_1 = \theta_2 = \pi/4$, however, the curves of $D(t)$ corresponding to various times overlap, and so the system is diffusive. This is a delocalization transition.

We attribute the delocalization at $\theta_1 = \theta_2 = \pi/4$ to the occurrence of a topological phase transition. In the absence of disorder, the quantum walk has topological invariants $(-1,0)$, and $(+1,0)$ at the end points of the path, respectively. It is thus plausible that somewhere along the path a topological phase transition has to occur. Our observations show that this transition occurs at the point $\theta_1 = \theta_2 = \pi/4$, which is also what one might expect on symmetry grounds.

Another angle from which to understand the delocalization at $\theta_1 = \theta_2 = \pi/4$ is the following. At the interface between two domains of the quantum walk with different topological phases there are edge states [19]. If both possible topological quantum numbers occur locally with equal probability, a

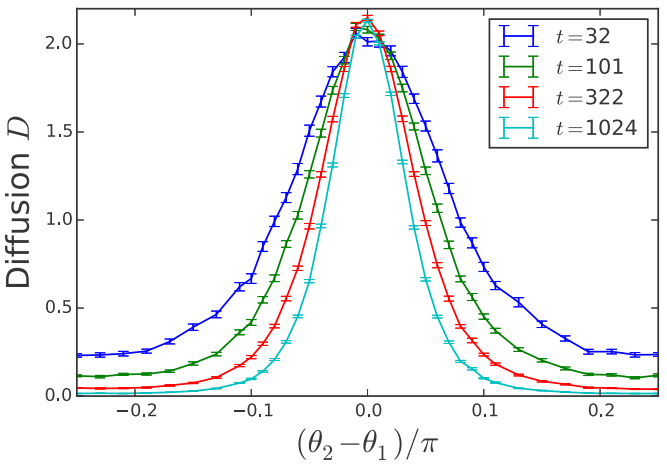

FIG. 4. (Color online) Diffusion coefficient as a function of $\theta_2 - \theta_1$ with $\theta_1 + \theta_2 = \pi/2$ for $\delta\theta = 0.2\pi$, $\delta\phi = 2\pi$, obtained by averaging over 100 disorder realizations on a 220×220 lattice.

percolating network of edge states appears. At $\theta_1 = \theta_2 = \pi/4$, the possible local values of θ_1 and θ_2 are shown by the red transparent box in Fig. 1. This network can be thought of as a realization of the Chalker-Coddington network model for the integer quantum Hall effect [23], tuned to the plateau transition point. At this point, a nonzero conductance appears, which in this case is signaled by a diffusively spreading wave function.

B. Scaling analysis of the localization-delocalization transition

In this section, we perform a scaling analysis of the transition at $\theta_1 = \theta_2 = \pi/4$, where the localization length ξ of Eq. (8) has to diverge. We use the same approach as for the corresponding transition in the quantum anomalous Hall effect [24]: we compute high-accuracy data for the diffusion coefficient $D(t)$, and then we fit these data assuming power-law divergence of the localization length and single-parameter scaling. We summarize the main ideas and the results here and relegate the details to the Appendix.

The split-step quantum walk with generic values of θ_1 and θ_2 has a phase-disorder-dependent localization length ξ, defined in Eq. (8). This quantity effectively determines how far the wave function may spread. At a topological transition, the localization length has to diverge (there is no length scale associated with diffusive, i.e., metallic propagation). We assume that this divergence happens as a power law, in analogy with the quantum Hall case [25]

$$\xi = A|\eta|^{-\nu}. \tag{12}$$

Here, η is the distance from the critical point, A is a constant of proportionality, and ν is the critical exponent [10]. When this transition is obtained as explained above, along the line $\theta_1 + \theta_2 = \pi/2$, the role of η is played by

$$\eta = \theta_2 - \theta_1. \tag{13}$$

Instead of measuring the localization length ξ directly [which would require a calculation of $D(t)$ up to much larger times], we find ν by assuming single-parameter scaling of the diffusion coefficient $D(t)$ of Eq. (11). Taking finite-time corrections [22] into account, we have

$$\ln D(t) = F(t^{1/2\nu}u) + t^{-y}G(t^{1/2\nu}u); \tag{14}$$

$$u = \eta + \mathcal{O}(\eta^2). \tag{15}$$

Here, the scaling functions $F(z)$, $G(z)$, and $u(z)$, as well as the exponents y and ν, are to be fitted to the numerical data. The quality of the fits will provide justification for the single-parameter scaling assumption.

We computed the high-accuracy data for the fitting procedure by simulating the quantum walk on an 800×800 lattice for varying number of time steps over many disorder realizations. A large number of disorder realizations were used for the runs at shorter times [4001, 4001, 2001, 1001 to obtain $D(t)$ at $t = 32, 80, 203, 512$, respectively], whereas due to self-averaging, fewer disorder realizations already provided enough accuracy for the runs at longer times (200 realizations for $t = 8192, 3250, 1290$). The resulting values of $D(t)$ were then fitted with the scaling ansatz [Eq. (14)] using a Taylor series expansion of the functions F, G, and u to various orders.

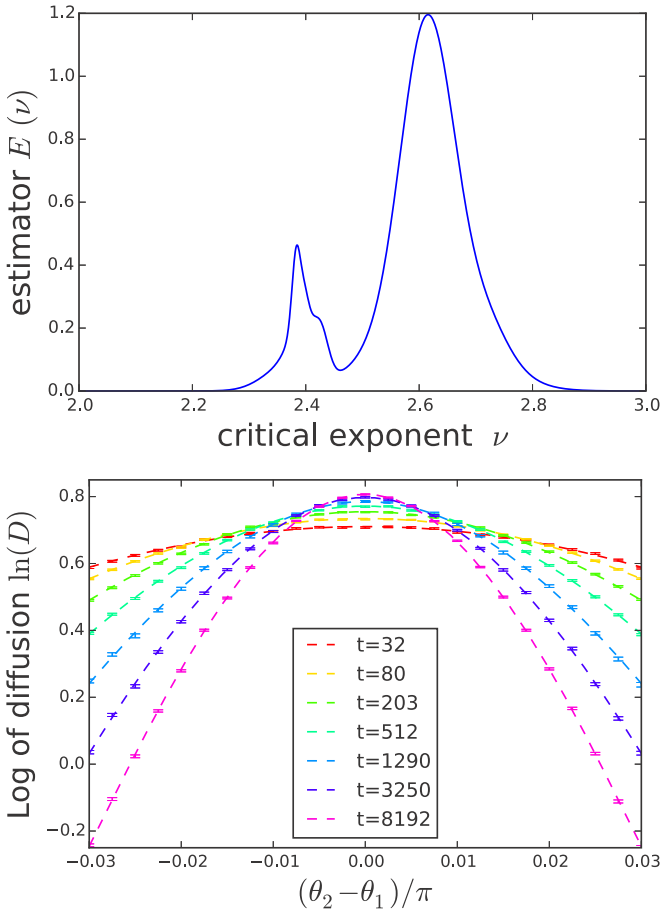

FIG. 5. (Color online) Top panel: estimator of critical exponent obtained. Rather than providing a histogram we have plotted the curve as a sum of 60 normalized Gaussians as given by Eq. (A5) ($N_{\max} = 60$). In the bottom panel, we show an example scaling fit to the diffusion coefficient data, demonstrating that the data for different t and $\theta_2 - \theta_1$ can be fitted to a single scaling function. Here, $J = 8$, $K = 3$, and $L = 1$ were chosen and $\nu = 2.592$ at $\xi^2/ndf = 0.94$ was obtained. The 68% confidence interval was found to be [2.557,2.625].

Instead of converging to a single solution, we obtained a good fit to the data for different forms of the scaling functions, and also different values of the exponents (an example is shown in Fig. 5, lower panel). To represent our estimate of the critical exponent ν, we define an estimator function $E(\nu)$, whose integral between any two values $\nu_{\min}$ and $\nu_{\max}$ reflects our degree of confidence that $\nu_{\min} < \nu < \nu_{\max}$. The construction of this function, along with the details of the fitting procedure, are explained in the Appendix.

As seen in Fig. 5, our estimator of the critical exponent ν is a bimodal function, with a peak around $\nu_m = 2.616$ (full width at half the maximum of 0.125), and a second peak at $\nu_2 = 2.384$. The value corresponding to the larger peak $\nu_m = 2.616$ is very close to the quantum Hall critical exponent [25] of 2.593 ± 0.003. The smaller peak is close to previous estimates of the exponent of the quantum Hall transition [10], which are now attributed to bistability of the fitting procedure, possibly related to finite-size effects [26]. To summarize, the transition

which we observe is compatible with the integer quantum Hall transition universality class.

IV. DISORDER IN THE ROTATION ANGLES OF THE SPLIT-STEP WALK

We already introduced disorder to the rotation angles of the split-step quantum walk, although with a small value of $\delta\theta = 0.2\pi$, in the previous sections. We now examine what happens to the quantum walk as this disorder grows. We first consider a split-step quantum walk that is localized by maximal phase disorder. As we turn on the angle disorder $\delta\theta$, we will find that at special values of $\delta\theta$, the walk delocalizes. We then consider a split-step walk with no phase disorder, only angle disorder. We find that, contrary to what one might expect, angle disorder does not induce localization.

A. Competition of phase and angle disorder: Disorder-induced delocalization

We now consider what happens if we first localize a quantum walk by phase disorder, as in Sec. II B, and then increase the disorder in the rotation angles $\delta\theta = \delta\theta_1 = \delta\theta_2$ to π. At this maximal value, as well as at $\delta\theta = \pi/2$, all inequivalent values of the rotation angles are equally likely. According to the network model pictured described in Sec. III A, we expect a percolating network of edge states and thus expect delocalized behavior at these values of the rotation angle disorder.

Our numerics clearly show the disorder-induced delocalization, at both $\delta\theta = \pi/2$ and π. We plot the time-dependent diffusion coefficient $D(t)$ in Fig. 6, as a function of $\delta\theta$, at fixed mean values of the rotation angles $\theta_1 = 0.35\pi$, $\theta_2 = 0.15\pi$, and maximal phase disorder $\delta\phi = 2\pi$. The diffusion coefficient decreases with time, indicating localized dynamics, except near the points of maximal disorder $\delta\theta = \frac{\pi}{2}$ and π: there, the system is diffusive.

We believe that the disorder-induced delocalization we observe here accompanies a topological phase transition, much like in the case of Fig. 4. Indeed, for $\delta\theta < \pi/2$ the majority of sites have parameters corresponding to topological invariants of $(+1,0)$, whereas for $\pi/2 < \delta\theta < \pi$, the majority topological invariant is $(-1,0)$. It is thus plausible that at $\delta\theta = \pi/2$, a topological phase transition occurs. We performed a scaling analysis on this transition, with now the control parameter being $\eta = \delta\theta - \pi/2$. We obtained consistent results of $\nu = 2.58 \pm 0.05$, in agreement with the mode of the distribution of $\nu_m = 2.6$ shown in Fig. 5. This confirms that the exponent ν is universal: its value does not depend on the method we use to drive the system across the transition.

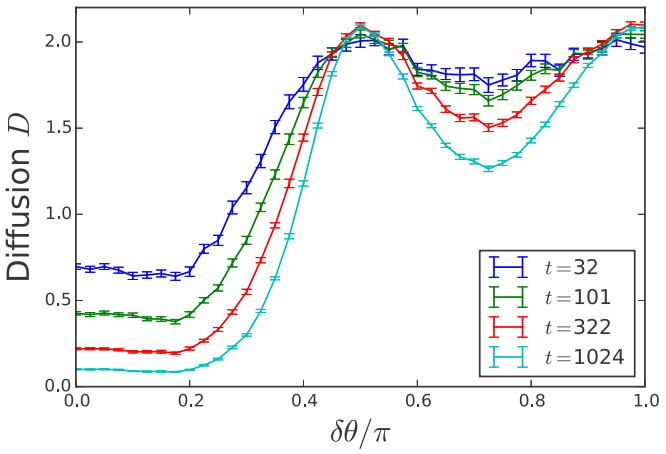

FIG. 6. (Color online) Diffusion coefficient as a function of $\delta\theta$ for $\delta\phi = 2\pi$, $\theta_1 = 0.35$, $\theta_2 = 0.15$, obtained by averaging over 100 disorder realizations on a 220×220 lattice.

B. Diffusive behavior in the presence of only rotation angle disorder

Finally, we investigate the spreading of the split-step quantum walk in the presence of only rotation angle disorder. We fix the mean rotation angles to $\theta_1 = 0.35\pi$ and $\theta_2 = 0.15\pi$. This choice of the mean rotation angles places the system in an insulating phase with topological invariants $(+1,0)$, as shown by the blue four-sided star in Fig. 1.

In Fig. 7, we show the result of increasing the rotation angle disorder from $\delta\theta = 0$ to 2π. We observe the expected ballistic behavior at $\delta\theta = 0$, and already for rather small values of $\delta\theta$ we see the crossover to the diffusive regime with $s \propto t^{1/2}$. Unlike in the case with phase disorder, though, we do not observe any signs of localization here.

Although we do not have a complete explanation for this absence of localization, we believe it is related to the particle-hole symmetry of the system, that is not broken by rotation angle disorder. The time-evolution operator has only real elements in position basis, and thus the effective Hamiltonian possesses particle-hole symmetry represented by complex conjugation. In time-independent lattice systems, the presence of this symmetry leads to nonuniversal behavior, and in some cases to diffusion instead of Anderson localization [10].

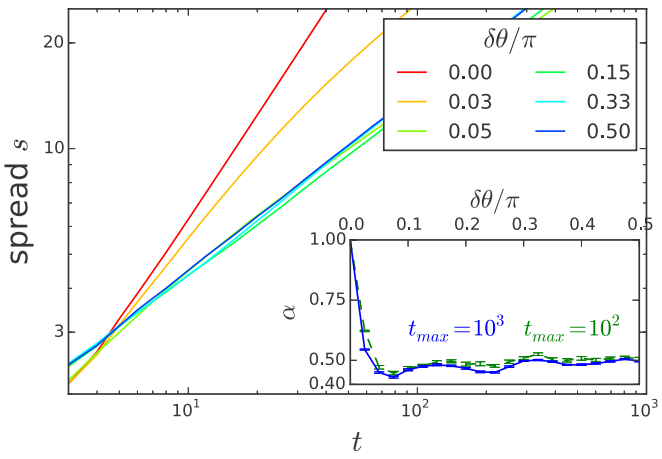

FIG. 7. (Color online) Spread of the quantum walker averaged over 100 disorder realizations for $\theta_1 = 0.35\pi$, $\theta_2 = 0.15\pi$ in the absence of phase disorder, as the angle disorder is increased from 0 to its maximal value of $\pi/2$. Just like Fig. 3, the inset shows the fitted power-law exponent of $s(t) \propto t^{\alpha}$. For large $\delta\theta$, we obtain a time independent $\alpha \approx \frac{1}{2}$, unlike in the case where phase disorder was present.

V. SUMMARY AND CONCLUSION

To summarize, we have found that the Hadamard walk is not localized by phase disorder, while generic split-step quantum walks are. We gave an intuitive physical explanation for this difference, namely, that the Hadamard walk is a split-step walk tuned to a topological phase transition. We corroborated this picture by numerically demonstrating that this transition can be reached through angle disorder as well, at precisely the value that this explanation predicts. We determined the critical exponent for the divergence of the localization length for both of these routes to criticality, and found $\nu = 2.6$, which places the split-step quantum walk with phase disorder in the universality class of the quantum Hall effect. We have also found that angle disorder alone does not localize the split-step quantum walk, which may be due to the fact that this disorder does not break the particle-hole symmetry of the system.

A useful next step to strengthen our interpretation of the localization effects of disorder would be the calculation of the topological invariant of the disordered split-step walk, the quasienergy winding. Here, any of the existing approaches to the Chern number in disordered systems can be of use. One could extend the definition of the quasienergy winding [20] using noncommutative geometry [27,28], or measure the winding number of the scattering matrix [24,29,30].

Another interesting question to pursue concerns at which point (and whether) the disorder-driven delocalization transition occurs for nonuniform disorder distributions, e.g., Gaussian disorder distributions for θ_1 and θ_2 or a binary distribution [with the two sets of (θ_1,θ_2) having different topological invariants].

Our interpretation of the localization phenomena relied on qualitative similarity with disordered quantum (anomalous) Hall insulators; we even obtained the same critical exponent. However, there are also ways in which these two disordered systems differ from each other. In the quantum anomalous Hall insulator study, a disorder-induced splitting of the transition from Chern number $+1$ to -1 into two transitions was observed [24]. In this paper, on the other hand, no such splitting of the transition from quasienergy winding $+1$ to -1 was found. To better understand these differences, perhaps the four-step walk [19] can help, as it can realize all possible combinations of trivial/nontrivial Chern number and quasienergy winding.

ACKNOWLEDGMENTS

We would like to acknowledge useful discussions with M. Rudner, C. Beenakker, and C. Fulga. We also acknowledge the use of the Leiden computing facilities. This work was funded by Nordita and also supported by the Hungarian National Office for Research and Technology under the Contract No. ERC_HU_09 OPTOMECH, by the Hungarian Academy of Sciences (Lendület Program, LP2011-016), and by by the Hungarian Scientific Research Fund (OTKA) under Contracts No. K83858 and No. NN109651.

APPENDIX: DETAILS OF THE SCALING ANALYSIS

We determine the critical exponent ν by a scaling analysis as used in Refs. [24,31], which will allow us to classify to which universality class this localization transition belongs. Instead of measuring the localization length ξ directly from the numerics, we assume single-parameter scaling, and determine ξ from the diffusion coefficient $D(t)$ of Eq. (11). The scaling law for the logarithm of the diffusion coefficient in dynamical localization [22] reads as[3]

$$\ln D(t) = \tilde{F}(\xi^{-2}t). \tag{A1}$$

Here, the scaling function $\tilde{F}(z)$ is some continuous, differentiable function of its argument z.

We insert the power-law diverging behavior for ξ, given by Eq. (12), into Eq. (A1), rescale the function $\tilde{F}$, and add finite-time corrections [22] to obtain

$$\ln D(t) = F(t^{1/2\nu}u) + t^{-y}G(t^{1/2\nu}u); \tag{A2}$$

$$u = \eta + \mathcal{O}(\eta^2). \tag{A3}$$

Here, the function F is related to $\tilde{F}$ as

$$F(z) = \tilde{F}(z^{2\nu}/A^2), \tag{A4}$$

where A is the constant from Eq. (12). The function G takes into account finite-time corrections, with y denoting the first subleading exponent. We expand the formulas for $\ln D$ and u of Eq. (A2) in Taylor series

$$\ln D = \sum_{j=0}^{J} f_j (t^{1/2\nu}u)^j + \sum_{k=1}^{K} t^{-y} g_k (t^{1/2\nu}u)^{k-1},$$

$$u = \eta + \sum_{l=3}^{L} u_l \eta^l.$$

Since the function $\ln D$ must be even, j may only take even values. In contrast, k and l may only take odd values, although $k = 0$ is also allowed, $k = 0$ corresponding to the absence of finite-time corrections. We choose the order of the approximation by fixing $J,K,L \in \mathbb{N}$, and then fit the Taylor coefficients f_j, g_k, u_l, and the exponents y and ν to the $D(t)$ data. This allows us to obtain an estimate for the critical exponent ν.

We fitted the numerically obtained data for $D(t)$ with 90 different functions, defined by different values of $J \in \{2 \ldots 10\}$, $K \in \{0,1,3 \ldots 9\}$, and $L \in \{1,3,5\}$. In a first approach, we systematically increased the order of the approximation, i.e., the values of J, K, and L, until we obtained a reasonable goodness of fit. Unfortunately, this did not yield a uniform convergence, neither when the standard χ^2 test was used [value of χ^2 per degree of freedom (χ^2/ndf) of order 1], nor when the more sophisticated goodness of fit measure [32] Q was used. We thus resorted to an alternative approach, as explained following.

[3]We choose $\ln D$ instead of D to perform scaling on since this makes the fitting simpler, as only a lower-order expansion of the fitting function is required. This follows Ref. [24].

We represent our results for the critical exponent ν, by use of an estimator function $E(\nu)$, obtained by the following procedure. Out of the 90 different fitting functions $\mathcal{F}_i$, we reject those which gave a value of χ^2 outside of an acceptance range $0.5 < \chi^2/ndf < 2$. For the remaining 60 functions $\mathcal{F}_i$, with critical exponents ν_i, we used the bootstrap method to evaluate the goodness of fit Q_i, and the 68% confidence interval for the critical exponent: $\nu \in [\nu_i - \sigma_i^-, \nu_i + \sigma_i^+]$. The estimator $E(\nu)$ is then defined as

$$E(\nu) = \frac{1}{N_{\max}} \sum_{i=1}^{N_{\max}} \sqrt{2\pi\sigma_i} \exp\left(-\frac{(\nu-\nu_i)^2}{2\sigma_i^2}\right), \quad \text{(A5)}$$

with $N_{\max} = 60$, and $\sigma_i = (\sigma_i^+ + \sigma_i^-)/2$. This is the probability density of the critical exponent, if we deem all acceptable outcomes of our fitting procedure equally likely.

[1] J. Kempe, Contemp. Phys. **44**, 307 (2003).
[2] N. Shenvi, J. Kempe, and K. Birgitta Whaley, Phys. Rev. A **67**, 052307 (2003).
[3] V. Potoček, A. Gábris, T. Kiss, and I. Jex, Phys. Rev. A **79**, 012325 (2009).
[4] T. Kitagawa, E. Berg, M. Rudner, and E. Demler, Phys. Rev. B **82**, 235114 (2010).
[5] H. Obuse and N. Kawakami, Phys. Rev. B **84**, 195139 (2011).
[6] J. K. Asbóth, Phys. Rev. B **86**, 195414 (2012).
[7] M. Hasan and C. L. Kane, Rev. Mod. Phys. **82**, 3045 (2010).
[8] X.-L. Qi and S.-C. Zhang, Rev. Mod. Phys. **83**, 1057 (2011).
[9] T. Kitagawa, M. S. Rudner, E. Berg, and E. Demler, Phys. Rev. A **82**, 033429 (2010).
[10] F. Evers and A. D. Mirlin, Rev. Mod. Phys. **80**, 1355 (2008).
[11] L. K. Grover, Phys. Rev. Lett. **79**, 325 (1997).
[12] Y. Yin, D. E. Katsanos, and S. N. Evangelou, Phys. Rev. A **77**, 022302 (2008).
[13] A. Schreiber, K. N. Cassemiro, V. Potoček, A. Gábris, I. Jex, and C. Silberhorn, Phys. Rev. Lett. **106**, 180403 (2011).
[14] A. Ahlbrecht, V. B. Scholz, and A. H. Werner, J. Math. Phys. **52**, 102201 (2011).
[15] A. Joye, Quantum Inf. Proc. **11**, 1251 (2012).
[16] J. Ghosh, Phys. Rev. A **89**, 022309 (2014).
[17] J. Svozilík, R. de J. León-Montiel, and J. P. Torres, Phys. Rev. A **86**, 052327 (2012).
[18] N. Inui, Y. Konishi, and N. Konno, Phys. Rev. A **69**, 052323 (2004).
[19] J. K. Asboth and J. M. Edge, Phys. Rev. A **91**, 022324 (2015).
[20] M. S. Rudner, N. H. Lindner, E. Berg, and M. Levin, Phys. Rev. X **3**, 031005 (2013).
[21] E. Abrahams, P. W. Anderson, D. C. Licciardello, and T. V. Ramakrishnan, Phys. Rev. Lett. **42**, 673 (1979).
[22] G. Lemarié, J. Chabé, P. Szriftgiser, J. C. Garreau, B. Grémaud, and D. Delande, Phys. Rev. A **80**, 043626 (2009).
[23] J. T. Chalker and P. D. Coddington, J. Phys. C: Solid State Phys. **21**, 2665 (1988).
[24] J. P. Dahlhaus, J. M. Edge, J. Tworzydło, and C. W. J. Beenakker, Phys. Rev. B **84**, 115133 (2011).
[25] K. Slevin and T. Ohtsuki, Phys. Rev. B **80**, 041304 (2009).
[26] K. Slevin and T. Ohtsuki, Int. J. Mod. Phys. Conf. Ser. **11**, 60 (2012).
[27] E. Prodan, J. Phys. A: Math. Theor. **44**, 239601 (2011).
[28] M. B. Hastings and T. A. Loring, J. Math. Phys. **51**, 015214 (2010).
[29] I. C. Fulga, F. Hassler, and A. R. Akhmerov, Phys. Rev. B **85**, 165409 (2012).
[30] M. Pasek and Y. D. Chong, Phys. Rev. B **89**, 075113 (2014).
[31] J. M. Edge, J. Tworzydło, and C. W. J. Beenakker, Phys. Rev. Lett. **109**, 135701 (2012).
[32] W. H. Press, S. A. Teukolsky, W. T. Vetterling, and B. P. Flannery, *Numerical Recipes: The Art of Scientific Computing* (Cambridge University Press, Cambridge, UK, 2007).